Electronic Supplementary Information (ESI)

Silicon Nanowire-Ta_2O_5-NGQD heterostructure: An efficient photocathode for Photoelectrochemical hydrogen evolution

Sk Riyajuddin[1], Jenifar Sultana[1], Shumile Ahmed Siddiqui[1], Sushil Kumar[1], Damini Badhwar[1], Shyam Sundar Yadav[2], Saveena Goyal[1], Ananth Venkatesan[2], Suvankar Chakraverty[1] and Kaushik Ghosh[1]*

[1]Institute of Nano Science & Technology, Knowledge City, Sector-81, SAS Nagar, Mohali, 140306, Punjab, India

[2]Indian Institute of Science Education and Research, Knowledge City, Sector-81, SAS Nagar, Mohali, 140306, Punjab, India

***Corresponding Author email: kaushik@inst.ac.in**

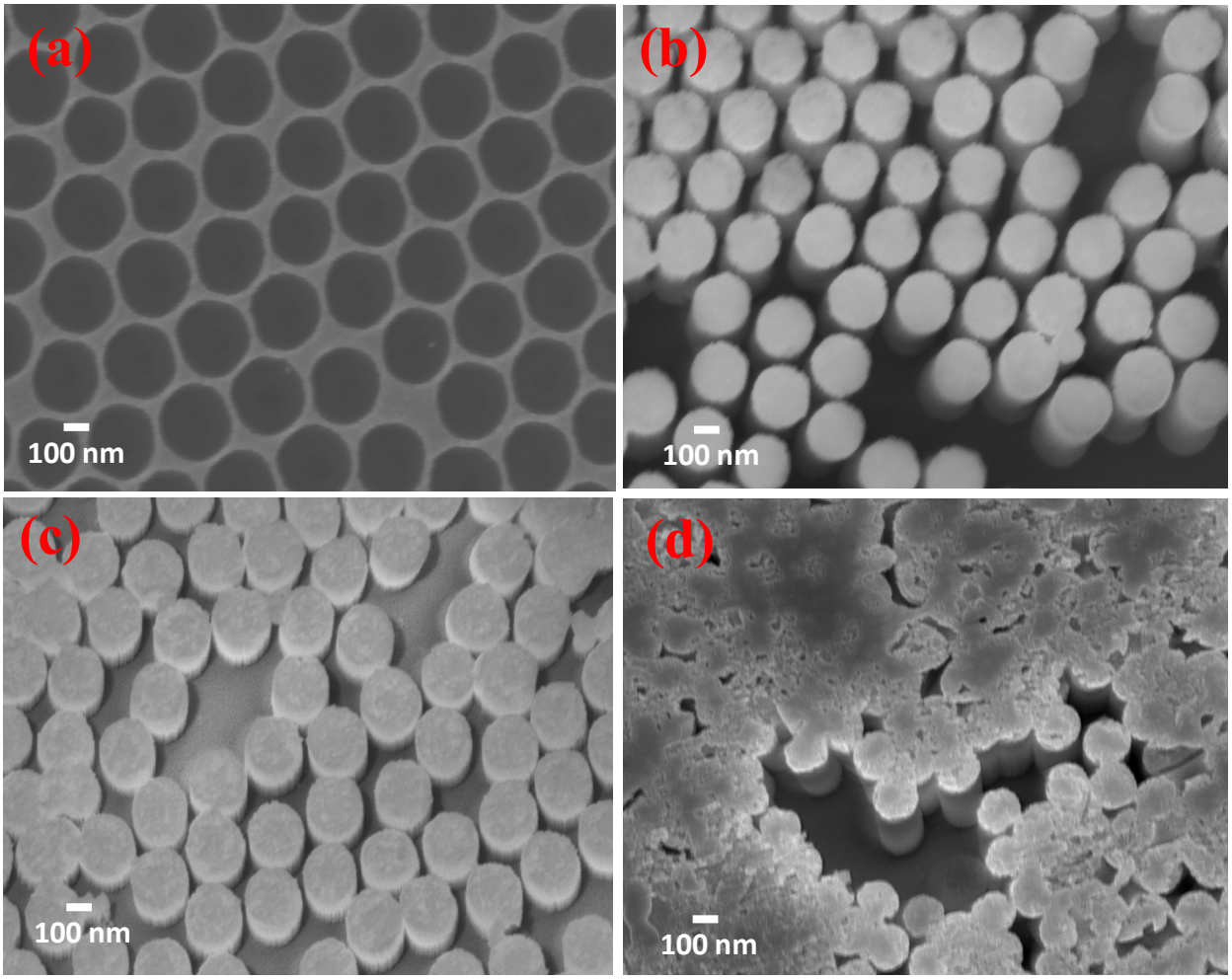

Figure S1. FE-SEM image of (a) hexagonal honeycomb-like gold mesh arrays after removal of PS beads on planar p-Si surface; p-SiNWs-Ta_2O_5 heterostructure with different thickness of Ta_2O_5 (b) 15 nm; (c) 40 nm; (d)80 nm.

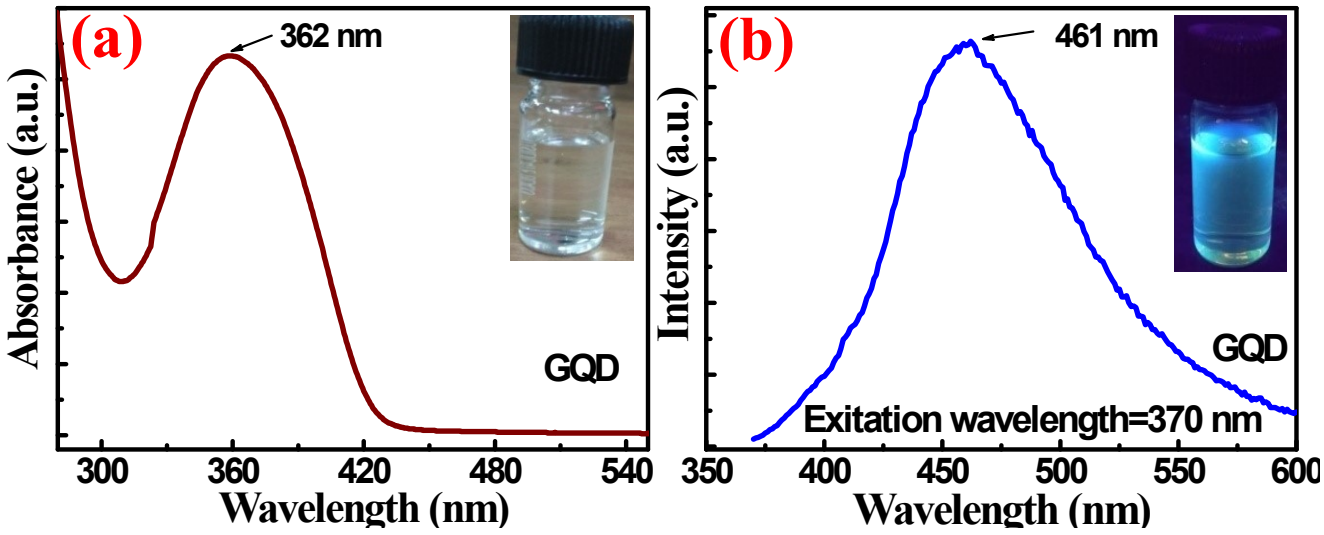

Figure S2. (a) Absorbance spectra and inset shows the solution colour under sunlight; (b) PL Spectra of GQD at an excitation wavelength of 370 nm and inset shows the solution colour under UV irradiation.

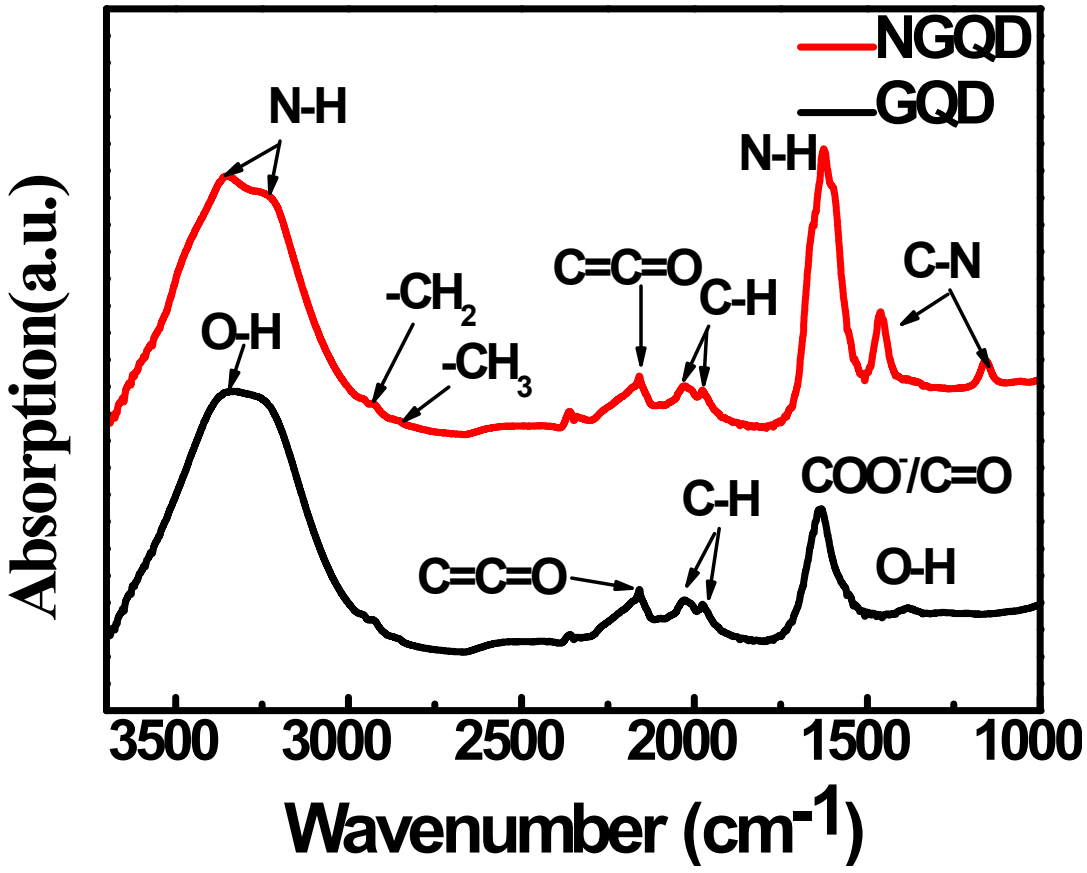

Figure S3. ATR-FTIR absorption spectrum corresponding to both GQD and NGQD. In GQD, the bands at 3329 and 1387 cm^{-1} corresponds to the vibration mode of O-H functional group. The absorption bands at 2925, 2856, 2159 and 2034 cm^{-1} indicate the stretching vibration mode of $-CH_2$, $-CH_3$, C=C=O and C=O bonds in both GQD and NGQD. Additionally, in NGQD, the newly formed bands at 3260~3132, 1625 cm^{-1} and; 1452, 1150 cm^{-1} corresponds to the bond formation of N-H and; C=N, C-N bonds, respectively.

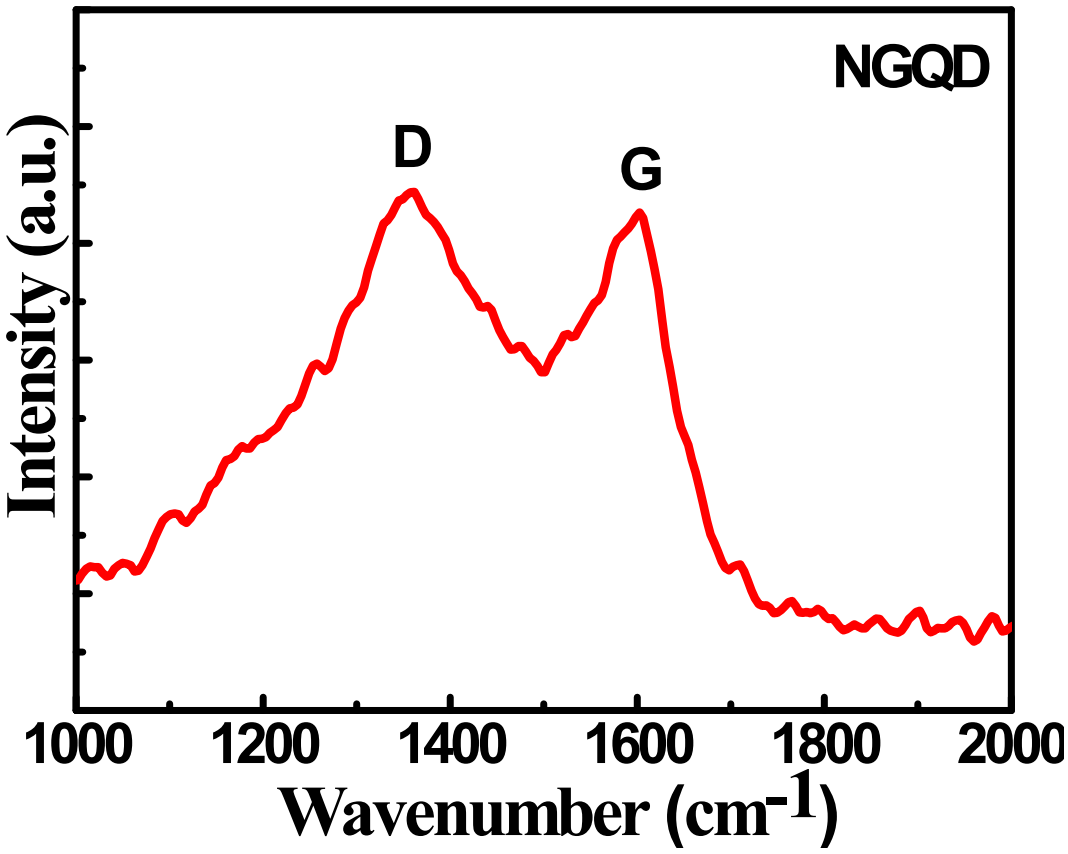

Figure S4. (a) Raman spectra of NGQD. The peaks centered at ~1365 and 1600 cm^{-1} corresponding to the D and G bands, which are attributed to the in-plane A_{1g} and E_{2g} mode of vibrations, respectively.

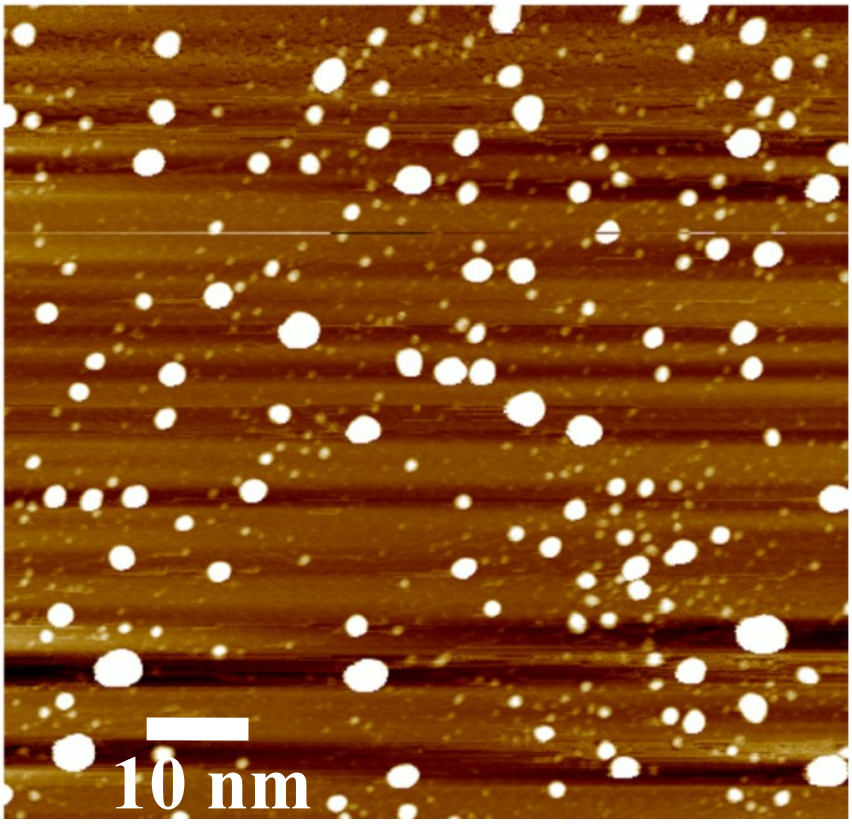

Figure S5. AFM image of as-prepared NGQD and the diameter is found to be in the range of 3-4 nm.

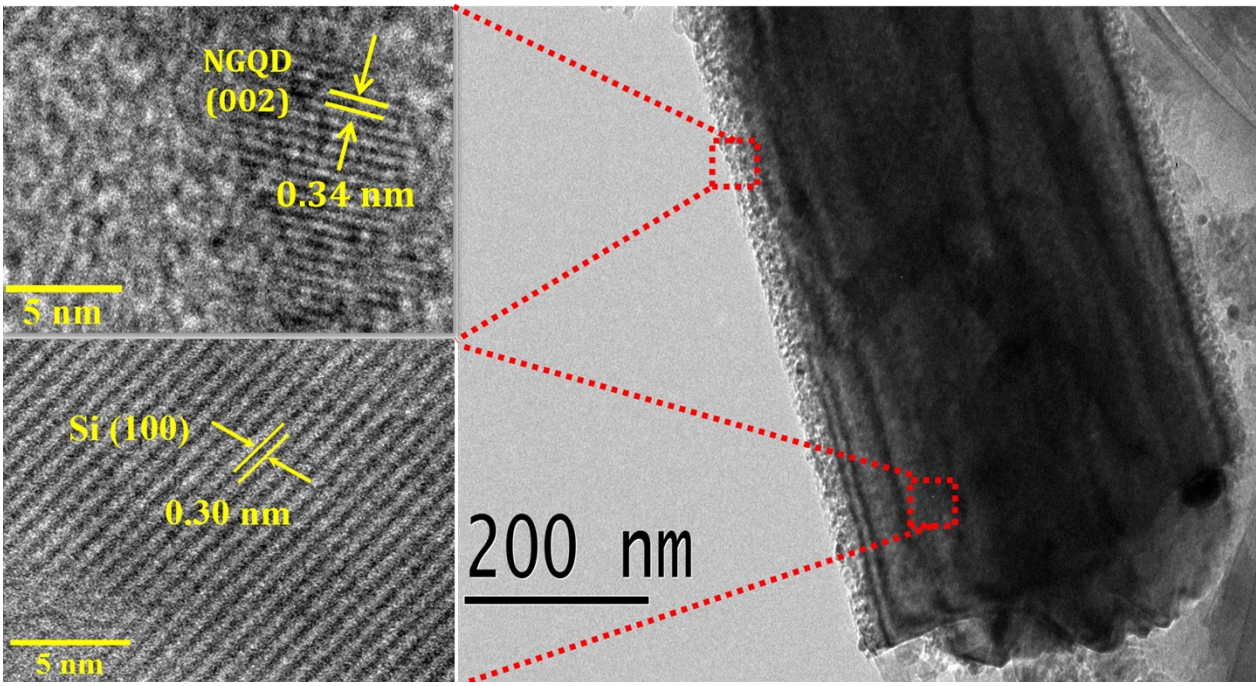

Figure S6. TEM image of p-SiNWs decorated with NGQD layer on its surface. HR-TEM images depicting the lattice fringes corresponding to both SiNWs ((100), d~ 0.30 nm) and NGQD ((002), d~ 0.34 nm), respectively.

Table S1. Calculated lattice spacing corresponding to Ta_2O_5 and Si from SAED pattern. where r represents the radius of the ring.

Label	1/2r (1/nm)	1/r (1/nm)	r (nm)
Si (100)	6.311	3.312	0.301907
Ta_2O_5 (111)	8.683	4.341	0.230335
Si (222)	12.612	6.306	0.158579
Si (331)	16.428	8.214	0.121743
Si (220)	19.548	9.774	0.102312

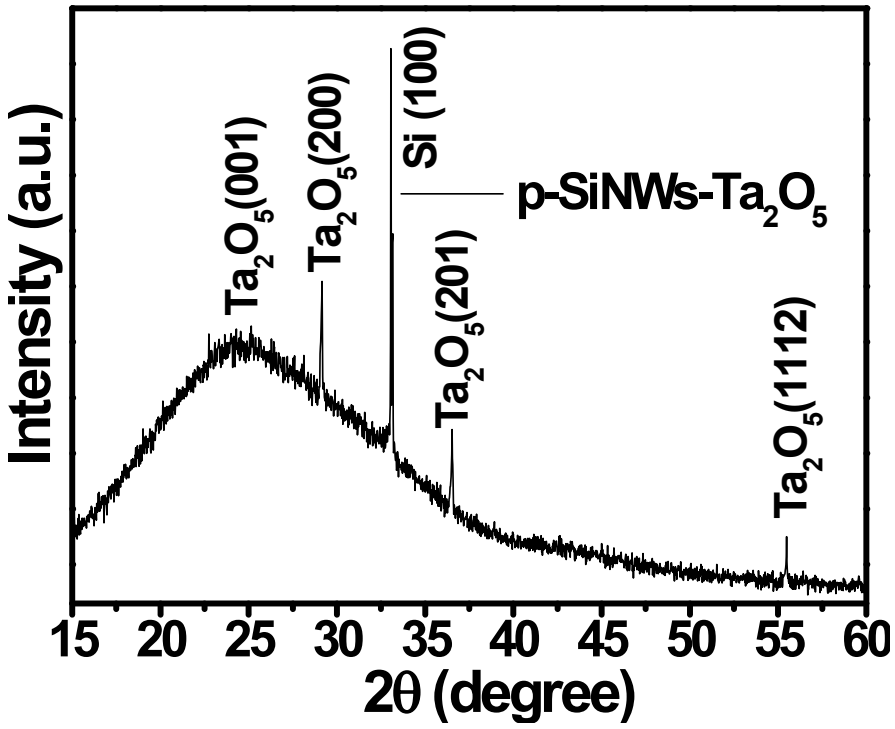

Figure S7. XRD analysis of p-SiNWs-Ta_2O_5 sample in where the diffraction peak at 23.81 29.16, 36.52, 55.52° corresponds to the lattice plans of (001), (200), (201) and (1112), respectively for Ta_2O_5 and 33.09° correspond to (100) plan of Si.

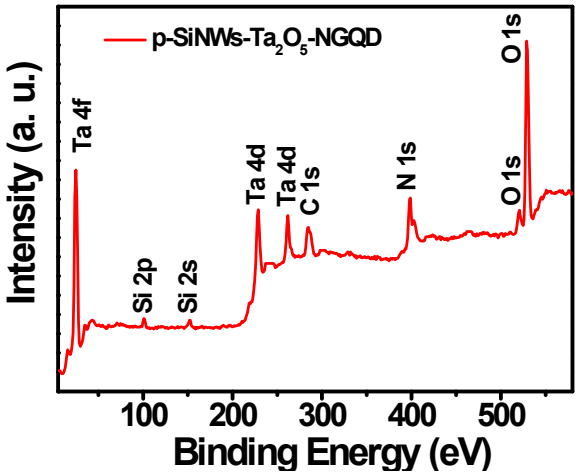

Figure S8. XPS Survey scan of p-SiNWs-Ta_2O_5-NGQD. The presence of all the elements (Si, Ta, O, N, C) confirms the formation of the heterostructure.

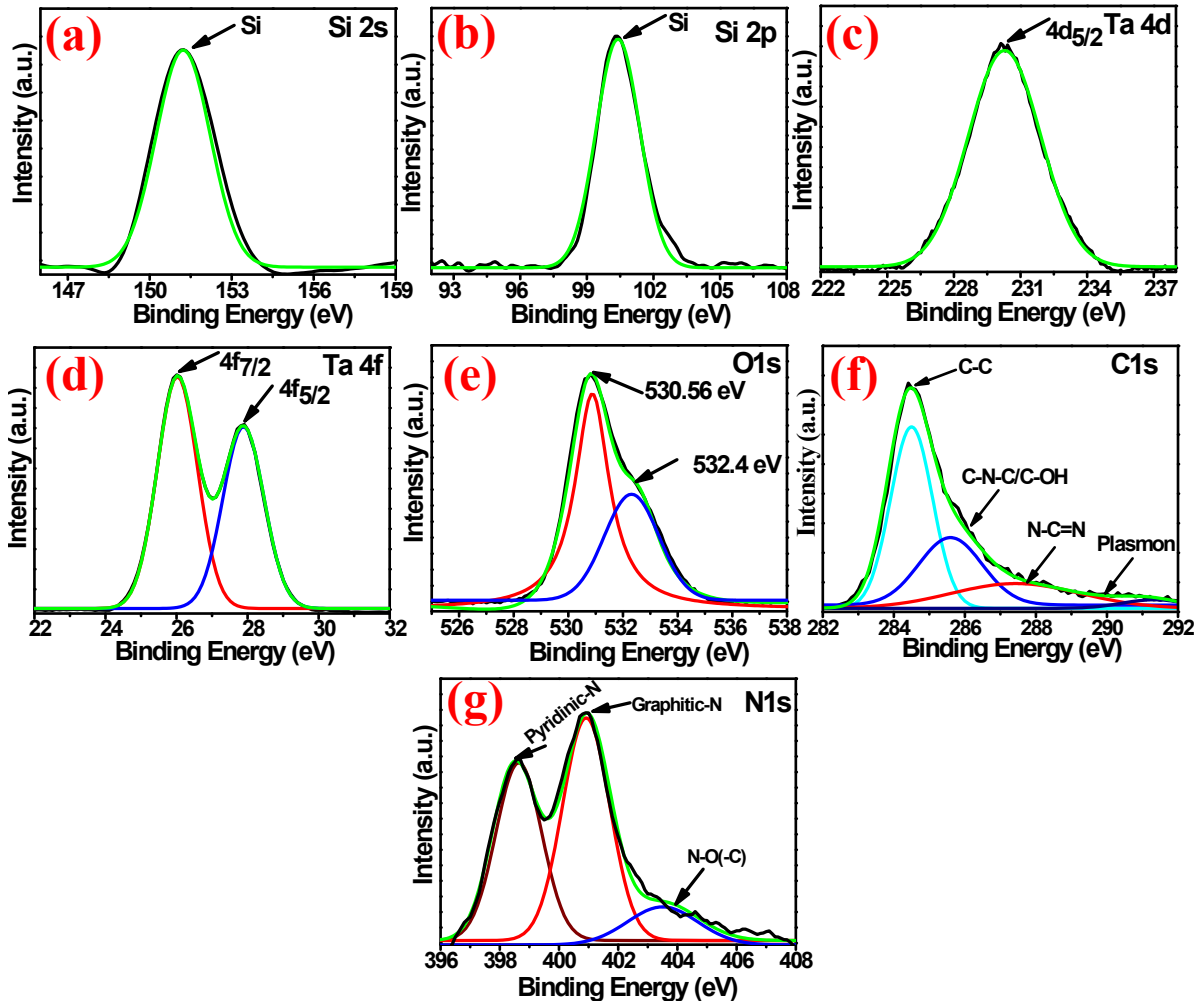

Figure S9. High-resulation XPS spectra of (a) Si 2s (b) Si 2p (c) Ta 4d (d) Ta 4f (e) O 1s (f) C1s (g) N1s of the prepared p-SiNWs-Ta_2O_5-NGQD heterostructure.

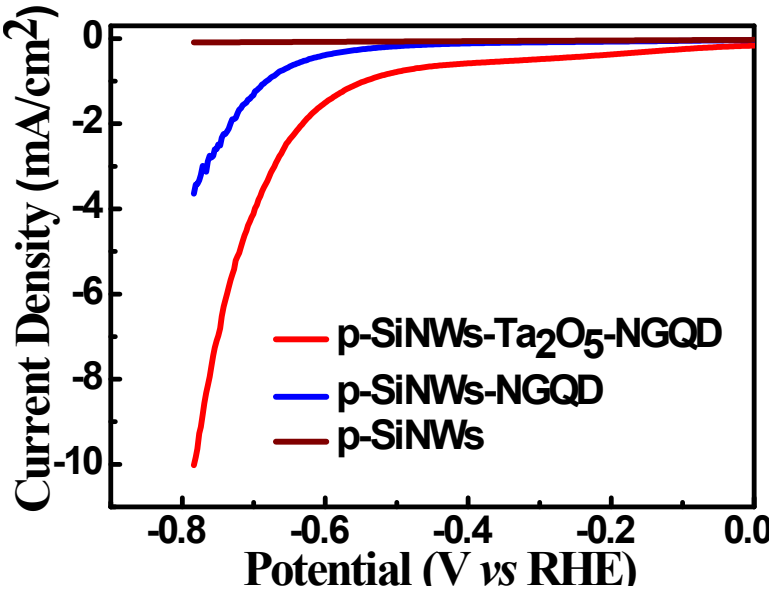

Figure S10. LSV polarization curve (without *iR* correction) for p-SiNWs, p-SiNWs-NGQD and p-SiNWs-Ta_2O_5-NGQD in 1 M $HClO_4$ solution in dark condition.

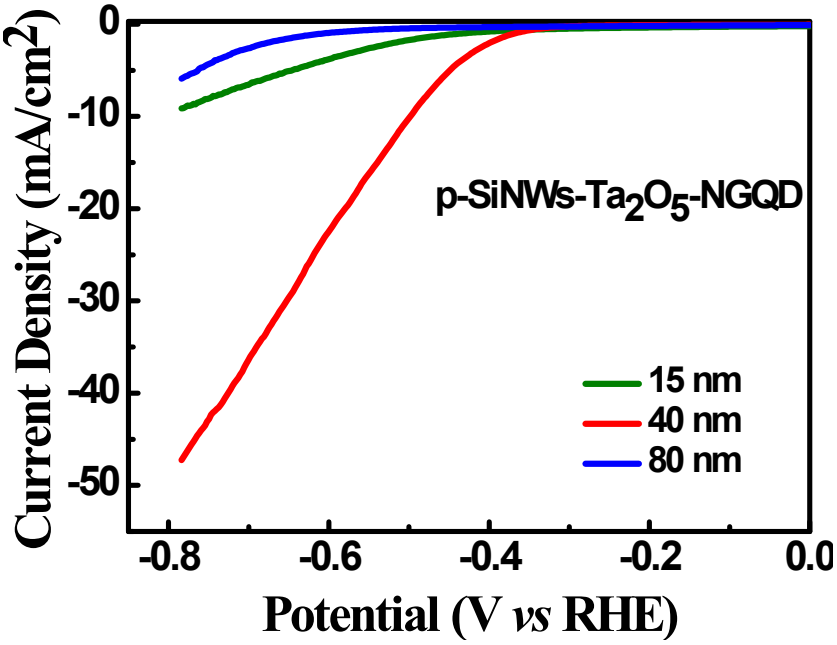

Figure S11. LSV polarization curve (without *iR* correction) for p-SiNWs-Ta_2O_5-NGQD in 1 M $HClO_4$ solution for different Ta_2O_5 thickness under illuminated condition.

Table S2. Comparison of PEC-HER performance in terms of overpotential, photocurrent density and ABPE of all as-grown samples in 1 M $HClO_4$ solution under illuminated and dark conditions, respectively.

Condition	**Working Electrode**	**Over-potential (mV)@5 mA/cm²**	**Over-potential (mV)@10 mA/cm²**	**Current density(mA/cm²) @ -0.78 V (*vs* RHE)**	**ABPE (%)**
Under illumination	p-SiNWs	-	-	-0.1	-
	p-SiNWs-NGQD	-745	-	-8.5	3.5
	p-SiNWs-Ta_2O_5-NGQD	-449	-498	-49.5	21.1
Under dark	p-SiNWs	-	-	-0.09	-
	p-SiNWs-NGQD	-	-	-3.64	-
	p-SiNWs-Ta_2O_5-NGQD	-720	-775	-10.05	-

Hydrogen evolution reaction (HER) mechanism in acid medium:

There are two different reaction mechanisms comprising of three steps for hydrogen evolution reaction (HER) under acidic medium. One is Volmer-Heyrovsky and the other is Volmer-Tafel, where the primary discharge step (Volmer step) is common in both the mechanism. The three steps for hydrogen evolution under acidic medium are as listed below.[1]

Step 1: Volmer reaction (Discharge step)

$$H_3O^+ + e^- + M \rightleftharpoons M\text{-}H_{ads} + H_2O;$$

In this step, the electrons move towards the cathode surface and concurrently there is a formation of M-H_{ads} intermediate state by the hydronium ions (H_3O^+) coming from the electrolyte side (where M is the active surface of the metal). Here, Tafel slope b ~ 120 mV.

Step 2: Heyrovsky reaction (desorption step)

$$M\text{-}H_{ads} + H_3O^+ + e^- \rightleftharpoons H_2 + M + H_2O;$$

In this step, the H_{ads} intermediates combine with a electron and hydronium ion and produce H_2 molecule, while the density of H_{ads} on the surface of the metal is very less and Tafel slope, b ~ 40 mV under such condition.

Step 3: Tafel reaction (Recombination Step)

$$M\text{-}H_{ads} + H_{ads}\text{-}M \rightleftharpoons H_2 + 2M;$$

This step occurs when there is a high density of H_{ads} on the metal surface, leading to the recombination of the two nearby H_{ads} intermediates together to form a H_2 molecule. Under such condition, Tafel slope b ~ 30 mV.

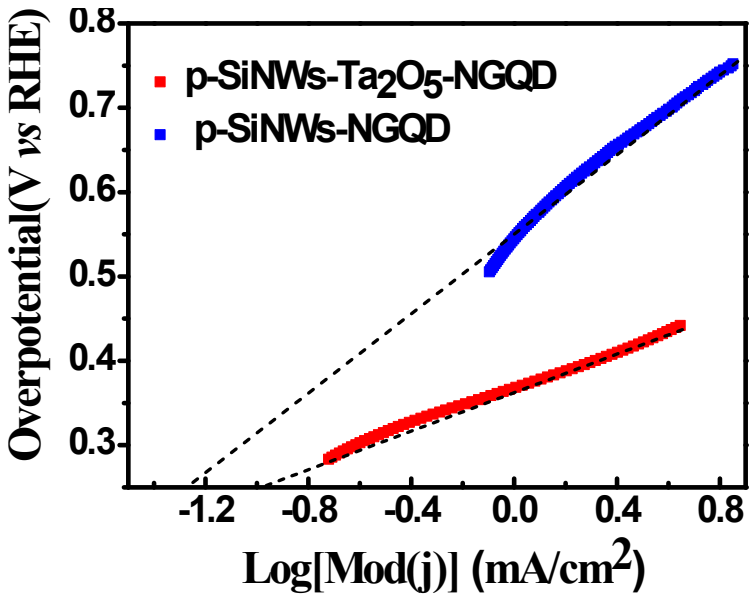

Figure S12. Calculated exchange current density of p-SiNWs-Ta_2O_5-NGQD and p-SiNWs-NGQD *via* extrapolating the Tafel plots to the X-axis under illumination

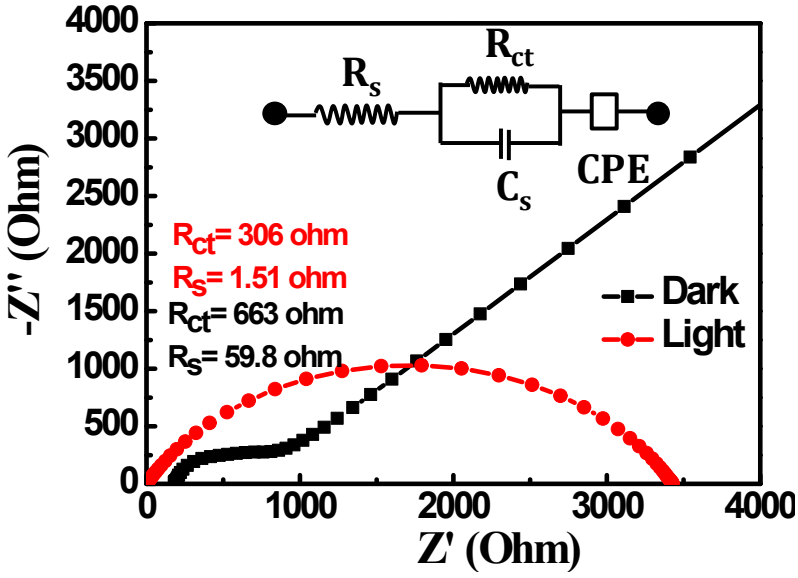

Figure S13. Nyquist plots of p-SiNWs-Ta_2O_5-NGQD in light and dark conditions in 1 M$HClO_4$ solution. Inset shows the fitted circuit diagram of the above Nyquist plots.

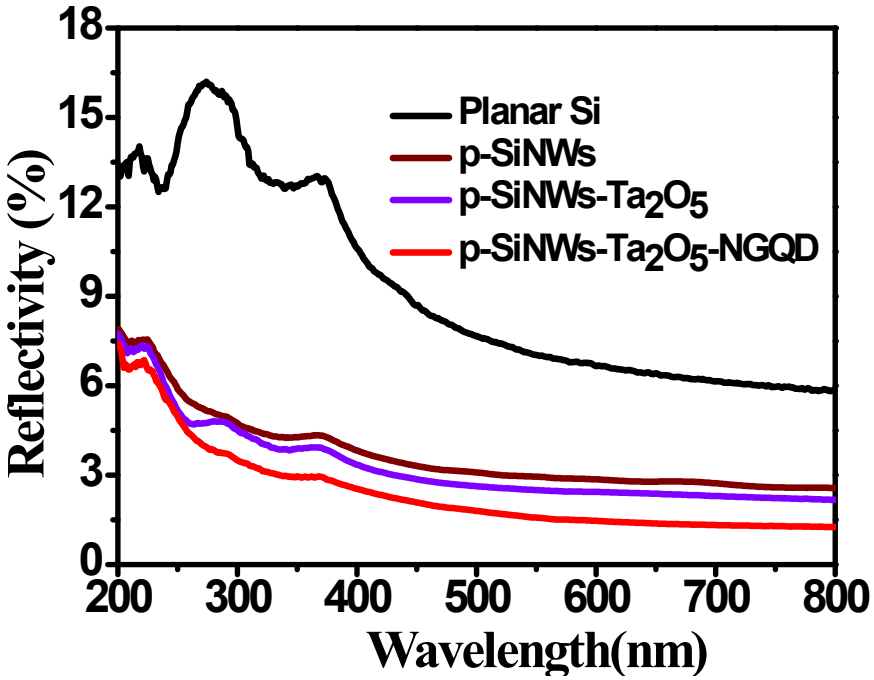

Figure S14. DRS UV-Vis spectra analysis of Planar Si, p-SiNWs, p-SiNWs-Ta_2O_5 and the p-SiNWs-Ta_2O_5-NGQD hetero-structure. The result shows the reflectivity decreases with the decoration of Ta_2O_5 and NGQD on top of the p-SiNWs as compared to planar Si substrate.

Table S3. The PEC-HER performance of the as-prepared p-SiNWs-Ta_2O_5-NGQD heterostructure in comparison with the recently reported Metal and Metal-Free Si-based photocathodes.

S. No	Material	Electrolyte	Photo current (mA/cm^2)	ABPE (%)	Over Potential (mV)@10 mA/cm^2	Ref.
1.	SiNW/Ni-B SiNW/Co-B	2M PBS	-15.6 -19.5	2.45 2.53	-54 -	2
2.	n^+p Si microwire /Ni-Mo n^+p Si microwire/Pt	KHP Buffer (pH=4)	-9.1 -13.2	1.9(STH) 2.7(STH)	-	3
3.	p-i-n Si/ Pt/Co_3O_4 n-i-p Si/ Pt/Co_3O_4	1M KOH 1M KOH	-12.03 -7.3	3.3 0.93	-	4
4.	Si-$SrTiO_3$(Ti/Pt catalyst)	0.5M H_2SO_4	-35	4.9	-	5
5.	pn^+-Si/Ta2O5/Pt	1 M $HClO_4$	-34.7	8.1	-	6
6.	Si/TaO_x	1 M HCl	-37.1	7.7	-	7
7.	SiNWs – MoS_2	0.5 M H_2SO_4	-26.5	1.05		8
8.	n^+p-Si/$MoSe_2$	1 M $HClO_4$	-29.3	3.8%	-195	9
9.	Si/MoS_2Cl	0.5MH_2SO_4	-20.6	-	-160	10
10.	ZnO/a-Si/TiO_2	0.5 M aqueous KHP	-11.6	5.5	-	11
11.	Si/TiO2/MoS2	0.5 M H_2SO_4	−0.24	-	-	12
12.	n^+p SiNWs/Pt	0.5 M K_2SO_4	-15	6.6	-	13
13.	Si /Al_2O_3 (Pt catalyst)	0.5M H_2SO_4	-26.2	-	-	14
14.	p-Si/SiO_2/Ti/Pt	0.5 M H_2SO_4	-22	2.9%	-	15
15.	n^+p-Si /TiO_2/Pt	1M $HClO_4$	-34.8	STH – 10.8	-	16
16.	n^+p-Si/Mo/MoS_2/Pt n^+pSi/Mo/MoS_2/MoS_x/Pt n^+p-Si/W/WS_2/Pt	1 M $HClO_4$	-10.9 -12 -9	- - -	-	17
17.	n^+p-Si/Co-S	0.5M H_2SO_4	-11	-	-85	18
18.	p-Si NW/Pt	H_2SO_4 + 0.5M K_2SO_4 (pH=1)	-20	-	-	19
19.	p-SiNWs/TiO_2/Pt	0.5M H_2SO_4	-30	-	-	20
20.	p-SiNWs/MoS_2	1M Na_2SO_4	-1	STH-0.03%	-	21
21.	n-type SiNWs/Bi_2O_3	1 M NaOH	-1.28	0.47	-	22
22.	SiNWs/CdSe QD	0.25M Na_2S + 0.35M Na_2SO_3	-6.1	-	-	23
23.	Si/PEDOT hybrid	1M KOH	-2.5	-	-	24

	core/shell NW array					
24.	SiNW/ $Fe_2S_2(CO)_6$	0.1M H_2SO_4	-17	-	-	25
25.	Vertically aligned SiNWs (n-type)	200 mM Me_2FcB_4 + 1M $LiClO_4$ in Ethanol.	4.19	-	-	26
26.	Si MWs/MoO_xS_y-10 Si MWs/MoO_xS_y-30 Si MWs/MoO_xS_y-50	0.5M K_2SO_4 + H_2SO_4	-1.28 -7.35 -9.83	STH- 0.05 0.63 0.82	-100	27
27.	Si MWs/$CoSe_2$	0.5 M Na_2SO_4 / H_2SO_4	-9	STH- 0.93	-320	28
28.	Si NWs/$Ni_{12}P_5$ Si NWs/Ni_2P	0.5 M H_2SO_4	-21 -22.6	STH- 2.97 STH- 3.13	-143	29
29.	Si NWs/Co-P	0.5M K_2SO_4 /H_2SO_4	-15.6	STH- 2.86	-	30
30.	Si NWs/FeP	0.5M K_2SO_4 /0.05M H_2SO_4	-13.9	STH- 2.64	-	31
31.	Si MWs/CoS_2 Si MWs/$CoSe_2$	0.5M H_2SO_4 1.0 M PBS	-3.22 -2.55	- -	-	32
32.	Si wires/WS_3 Si wires/WS_2	0.5M K_2SO_4/0.05M H_2SO_4	-19 -7	STH- 2.02 STH- 0.187	-670	33
33.	a-Si /Mo_2C	0.1 M H_2SO_4 1 M KOH	-11.2 -11.4	- -	-	34
34.	Pyramidal p-SiNWs-Co_2P	0.5 M H_2SO_4	-35.2	-	-	35

Metal Free Si based PEC-HER

1.	Graphene/Si	1M $HClO_4$	-31.1	0.32		36
2.	SiNW@N-doped GQS	1M $HClO_4$	-35	2.29	-	37
3.	N-doped monolayer Graphene/ Silicon	1M $HClO_4$	-5.5	STH-3.05	-	38
4.	rGO-SiNWs	1M $HClO_4$	-23.152	STH- 3.16	-	39
5.	Chl/CQDs-SiNWs	0.5M H_2SO_4	-26.36	7.86	-	40
6.	p-i-n SiNWs/NGQD	0.5 M H_2SO_4	-26.2	16.4	-460	41
7.	**p-SiNWs-Ta_2O_5-NGQD**	**1M $HClO_4$**	**-49.5**	**21.1**	**-498**	**This Work**

#ABPE- Applied Bias Photon-to-Current Efficiency
#STH- Solar to Hydrogen Conversion Efficiency

Mott-Schottky analysis:

The dependence of the inverse square capacitance of the space-charge region under reverse-bias in the semiconductor is given by the Mott-Schottky relation:[42]

$$\frac{1}{C_{sc}^2} = \frac{2}{\epsilon_0 \epsilon_{Si} q N_d}(V - E_{fb} - \frac{kT}{q}) \text{ ………………… (1)}$$

where ϵ_{Si} : Relative permittivity of Si (11.7), $\epsilon = \epsilon_{Si}\epsilon_0$

$\epsilon_0 = 8.85x10^{-14}$ F/cm

q: Elementary charge (1.6×10^{-19} C),

N_d : Donor concentration in the semiconductor,

V: potential difference between the semiconductor and the redox potential of the solution.

E_{fb} : Flat band potential,

K: Boltzmann's constant (1.38×10^{-27} cm^2 kg s^{-2} K^{-1})

T: Temperature (298 K).

The E_{fb} is determined by taking the value of the X-axis intercept of the extrapolated linear region of the $(C^{SC})^{-2}$ in the Mott-Schottky plot.

The barrier height φ_b is calculated using the Schottky's relation:

$$\varphi_b = E_{fb} + V_n \text{…………………………...(2)}$$

Where V_n is the difference between the potential of the conduction band edge and the Fermi level, and is obtained by using the following relationship

$$V_n = \frac{kT}{q}(\ln \frac{N_c}{N_d}) \text{…………………………..(3)}$$

The density of conduction band states (N_c) is calculated by:

$$N_c = 2\left(\frac{2\pi m_e^* kT}{h^2}\right)^{3/2} \quad \text{.....(4)}$$

where m_e^* : Effective mass of electron in Si ($m_e^* \sim 9.84\times10^{-31}$kg)

h: Planck's constant (6.63×10^{-34} Js).

Using the slope (slope $Slope = \frac{2}{q\epsilon N_D}$) of Mott-Schottky plot and the above equations, the $N_d$and $V_n$the are calculated.

Table S4. Calculated values of carrier concentration, flat band potential, barrier height of p-SiNWs, p-SiNWs-NGQD and p-SiNWs- Ta_2O_5 and p-SiNWs- Ta_2O_5-NGQD photocathodes from the Mott-Schottky analysis.

Working electrode	**N_c(cm^{-3})**	**N_d(cm^{-3})**	**E_{fb}(V)**	**V_n(V)**	**Φ_b(V)**
p-SiNWs-Ta_2O_5-NGQD	27.72e18	4.19e17	-0.78	0.11	-0.67
p-SiNWs-Ta_2O_5	27.72e18	1.8e17	-0.29	0.15	-0.14
p-SiNWs-NGQD	27.72e18	6.67e16	0.12	0.1	0.22
p-SiNWs	27.72e18	1.06e17	0.07	0.13	0.20

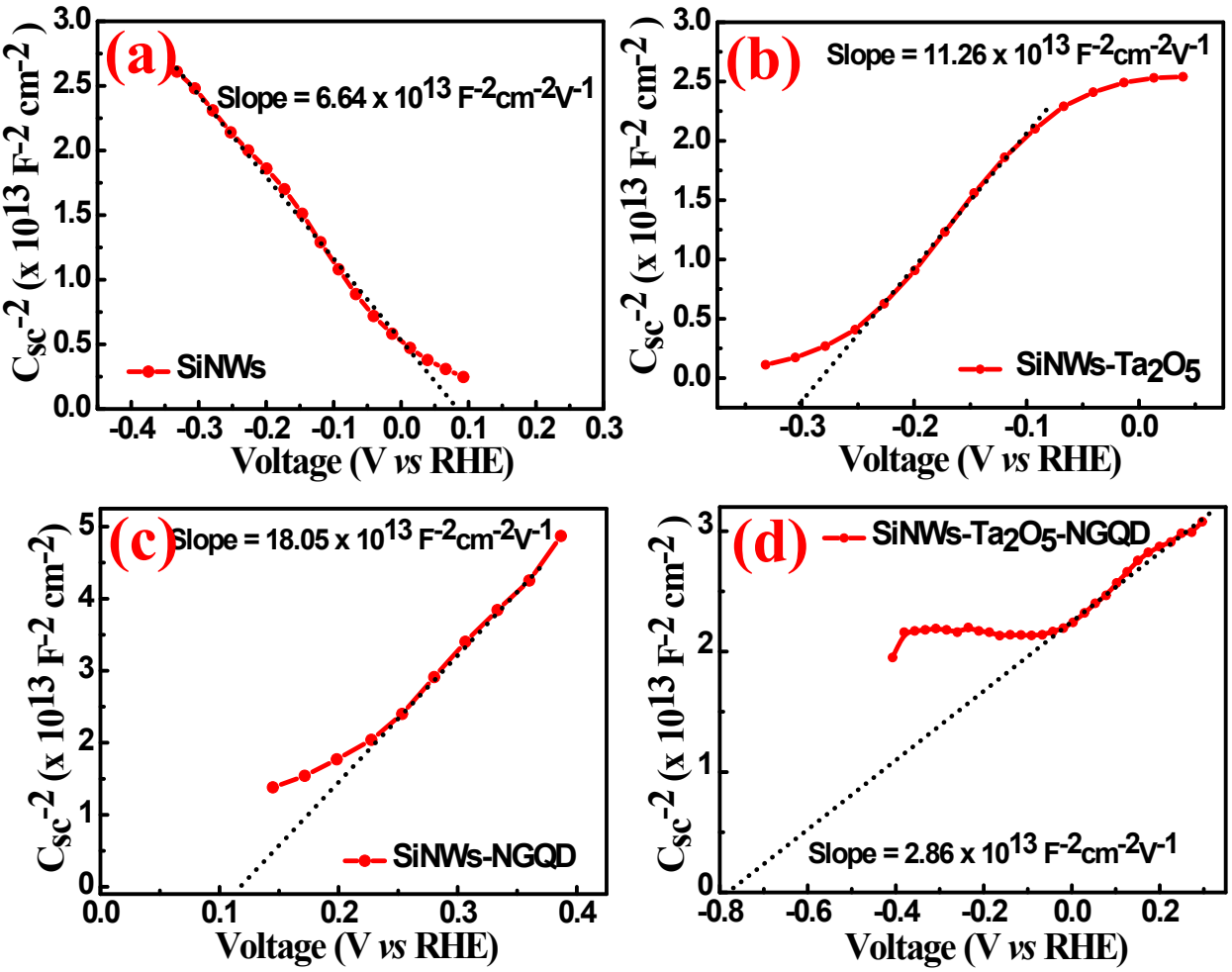

Figure S15. Mott-Schottky result of bare p-SiNWs, p-SiNWs-NGQD and p-SiNWs- $Ta_2O_5$and p-SiNWs- Ta_2O_5-NGQD photocathodes.

References:

1 S. Riyajuddin, K. Azmi, M. Pahuja, S. Kumar, T. Maruyama, C. Bera and K. Ghosh, *ACS Nano*, 2021, **15**, 5586–5599.
2 Y. Yang, M. Wang, P. Zhang, W. Wang, H. Han and L. Sun, *ACS Appl. Mater. Interfaces*, 2016, **8**, 30143–30151.
3 E. L. Warren, J. R. McKone, H. A. Atwater, H. B. Gray and N. S. Lewis, *Energy Environ. Sci.*, 2012, **5**, 9653–9661.
4 D. Zhang, Y. Cao, S. K. Karuturi, M. Du, M. Liu, C. Xue, R. Chen, P. Wang, J. Zhang, J. Shi and S. F. Liu, *ACS Appl. Energy Mater.*, 2020, **3**, 4629–4637.
5 L. Ji, M. D. McDaniel, S. Wang, A. B. Posadas, X. Li, H. Huang, J. C. Lee, A. A. Demkov, A. J. Bard, J. G. Ekerdt and E. T. Yu, *Nature Nanotech*, 2015, **10**, 84–90.
6 T. Wang, S. Liu, H. Li, C. Li, Z. Luo and J. Gong, *Ind. Eng. Chem. Res.*, 2019, **58**, 5510–5515.
7 Y. Wan, S. K. Karuturi, C. Samundsett, J. Bullock, M. Hettick, D. Yan, J. Peng, P. R. Narangari, S. Mokkapati, H. H. Tan, C. Jagadish, A. Javey and A. Cuevas, *ACS Energy Lett.*, 2018, **3**, 125–131.
8 G. Paulraj, P. S. Venkatesh, P. Dharmaraj, S. Gopalakrishnan and K. Jeganathan, *International Journal of Hydrogen Energy*, 2020, **45**, 1793–1801.
9 G. Huang, J. Mao, R. Fan, Z. Yin, X. Wu, J. Jie, Z. Kang and M. Shen, *Appl. Phys. Lett.*, 2018, **112**, 013902.
10 X. Zhang, F. Meng, S. Mao, Q. Ding, M. J. Shearer, M. S. Faber, J. Chen, R. J. Hamers and S. Jin, *Energy Environ. Sci.*, 2015, **8**, 862–868.
11 Y. Lin, C. Battaglia, M. Boccard, M. Hettick, Z. Yu, C. Ballif, J. W. Ager and A. Javey, *Nano Lett.*, 2013, **13**, 5615–5618.
12 X. Li, Y. Li, H. Wang, H. Miao, H. Zhu, X. Liu, H. Lin and G. Shi, *ACS Appl. Energy Mater.*, 2021, **4**, 730–736.
13 S. W. Boettcher, E. L. Warren, M. C. Putnam, E. A. Santori, D. Turner-Evans, M. D. Kelzenberg, M. G. Walter, J. R. McKone, B. S. Brunschwig, H. A. Atwater and N. S. Lewis, *J. Am. Chem. Soc.*, 2011, **133**, 1216–1219.
14 M. J. Choi, J.-Y. Jung, M.-J. Park, J.-W. Song, J.-H. Lee and J. H. Bang, *J. Mater. Chem. A*, 2014, **2**, 2928–2933.
15 D. V. Esposito, I. Levin, T. P. Moffat and A. A. Talin, *Nat Mater*, 2013, **12**, 562–568.
16 R. Fan, W. Dong, L. Fang, F. Zheng and M. Shen, *J. Mater. Chem. A*, 2017, **5**, 18744–18751.
17 A. B. Laursen, T. Pedersen, P. Malacrida, B. Seger, O. Hansen, P. C. K. Vesborg and I. Chorkendorff, *Phys. Chem. Chem. Phys.*, 2013, **15**, 20000–20004.
18 Y. Sun, C. Liu, D. C. Grauer, J. Yano, J. R. Long, P. Yang and C. J. Chang, *J. Am. Chem. Soc.*, 2013, **135**, 17699–17702.
19 I. Oh, J. Kye and S. Hwang, *Nano Lett.*, 2012, **12**, 298–302.
20 N. P. Dasgupta, C. Liu, S. Andrews, F. B. Prinz and P. Yang, *J. Am. Chem. Soc.*, 2013, **135**, 12932–12935.
21 P. D. Tran, S. S. Pramana, V. S. Kale, M. Nguyen, S. Y. Chiam, S. K. Batabyal, L. H. Wong, J. Barber and J. Loo, *Chemistry – A European Journal*, 2012, **18**, 13994–13999.
22 B. Weng, F. Xu and J. Xu, *Nanotechnology*, 2014, **25**, 455402.
23 R. R. Devarapalli, C. K. Kamaja and M. V. Shelke, *J. Mater. Chem. A*, 2014, **2**, 13352–13358.
24 X. Li, W. Lu, W. Dong, Q. Chen, D. Wu, W. Zhou and L. Chen, *Nanoscale*, 2013, **5**, 5257–5261.
25 S. Chandrasekaran, T. Nann and N. H. Voelcker, *Nanomaterials (Basel)*, 2016, **6**, 144.

26 G. Yuan, H. Zhao, X. Liu, Z. S. Hasanali, Y. Zou, A. Levine and D. Wang, *Angewandte Chemie*, 2009, **121**, 9860–9864.
27 X.-Q. Bao, D. Y. Petrovykh, P. Alpuim, D. G. Stroppa, N. Guldris, H. Fonseca, M. Costa, J. Gaspar, C. Jin and L. Liu, *Nano Energy*, 2015, **16**, 130–142.
28 M. Basu, Z.-W. Zhang, C.-J. Chen, P.-T. Chen, K.-C. Yang, C.-G. Ma, C. C. Lin, S.-F. Hu and R.-S. Liu, *Angewandte Chemie International Edition*, 2015, **54**, 6211–6216.
29 Z. Huang, Z. Chen, Z. Chen, C. Lv, H. Meng and C. Zhang, *ACS Nano*, 2014, **8**, 8121–8129.
30 X.-Q. Bao, M. F. Cerqueira, P. Alpuim and L. Liu, *Chem. Commun.*, 2015, **51**, 10742–10745.
31 C. Lv, Z. Chen, Z. Chen, B. Zhang, Y. Qin, Z. Huang and C. Zhang, *J. Mater. Chem. A*, 2015, **3**, 17669–17675.
32 C.-J. Chen, K.-C. Yang, M. Basu, T.-H. Lu, Y.-R. Lu, C.-L. Dong, S.-F. Hu and R.-S. Liu, *ACS Appl. Mater. Interfaces*, 2016, **8**, 5400–5407.
33 Z. Huang, C. Wang, Z. Chen, H. Meng, C. Lv, Z. Chen, R. Han and C. Zhang, *ACS Appl. Mater. Interfaces*, 2014, **6**, 10408–10414.
34 C. G. Morales-Guio, K. Thorwarth, B. Niesen, L. Liardet, J. Patscheider, C. Ballif and X. Hu, *J. Am. Chem. Soc.*, 2015, **137**, 7035–7038.
35 S. M. Thalluri, B. Wei, K. Welter, R. Thomas, V. Smirnov, L. Qiao, Z. Wang, F. Finger and L. Liu, *ACS Energy Lett.*, 2019, **4**, 1755–1762.
36 U. Sim, J. Moon, J. Lee, J. An, H.-Y. Ahn, D. J. Kim, I. Jo, C. Jeon, S. Han, B. H. Hong and K. T. Nam, *ACS Appl. Mater. Interfaces*, 2017, **9**, 3570–3580.
37 U. Sim, J. Moon, J. An, J. H. Kang, S. E. Jerng, J. Moon, S.-P. Cho, B. H. Hong and K. T. Nam, *Energy Environ. Sci.*, 2015, **8**, 1329–1338.
38 U. Sim, T.-Y. Yang, J. Moon, J. An, J. Hwang, J.-H. Seo, J. Lee, K. Y. Kim, J. Lee, S. Han, B. H. Hong and K. T. Nam, *Energy Environ. Sci.*, 2013, **6**, 3658–3664.
39 Y. Sim, J. John, J. Moon and U. Sim, *Applied Sciences*, 2018, **8**, 2046.
40 K. Roy, D. Ghosh, K. Sarkar, P. Devi and P. Kumar, *ACS Appl. Mater. Interfaces*, 2020, **12**, 37218–37226.
41 S. Riyajuddin, S. Kumar, D. Badhwar, S. A. Siddiqui, J. Sultana and K. Ghosh, *Sustainable Energy Fuels*,2021, **5**, 3160-3171.
42 I. A. Digdaya, G. W. P. Adhyaksa, B. J. Trześniewski, E. C. Garnett and W. A. Smith, *Nat Commun*, 2017, **8**, 15968.